

**Stability of solutal advective flow in a horizontal shallow layer**Aleksey Mizev,<sup>\*</sup> Elena Mosheva, and Konstantin Kostarev*Institute of Continuous Media Mechanics, Academica Koroleva Street 1, 614013 Perm, Russia*Vitaly Demin<sup>†</sup> and Eugenii Popov*Perm State University, Bukireva Street 1, 614990 Perm, Russia*

(Received 10 March 2017; published 20 October 2017)

This paper presents an experimental and numerical study on the structure and stability of a solutal advective flow in a horizontal shallow layer. The flow is induced by the initial longitudinal steplike density distribution caused by inhomogeneous solute concentration. It is shown that, when the density difference or the channel thickness increases, the main flow instability in the form of longitudinal convective rolls occurs in the near-wall region. This phenomenon originates from the Rayleigh-Taylor instability, which develops near both the upper and lower horizontal boundaries, where the unstable density stratification occurs due to no-slip boundary conditions. It is established that the solutal Péclet number, a measure of the relative strength of advection and diffusion, must exceed the critical value  $Pe^* \approx 300$  for the instability to set in. Moreover, the Péclet number uniquely determines the spatiotemporal characteristics of the secondary flow, namely, its wavelength and formation time. The results of the laboratory experiments are in good agreement with the numerical predictions.

DOI: [10.1103/PhysRevFluids.2.103903](https://doi.org/10.1103/PhysRevFluids.2.103903)**I. INTRODUCTION**

Advective flow arises in liquids and gases in a gravity field in the presence of a horizontal density gradient. This type of flow has attracted attention because of a variety of applications in meteorology, oceanography, geology, and crystal growth technologies. From a fundamental point of view, the advective flow is interesting as an example of the hydrodynamic system exhibiting a wide range of instabilities, which depend on liquid parameters and problem geometry.

The density gradient which triggers the flow can be caused by an inhomogeneous temperature or concentration distribution in binary liquids. A thermal problem for the case when an advective flow appears due to the presence of a longitudinal temperature gradient has been investigated in a large number of theoretical [1–11] and experimental [12–15] works. In a horizontal shallow layer, the main flow becomes unstable with respect to two different types of instabilities, which are related to the Prandtl number. The instability of hydrodynamic origin caused by the shear between the counterflows develops at low Prandtl numbers corresponding to liquid metals. At high Prandtl numbers the Rayleigh-Taylor instability becomes more dangerous, leading to the development of longitudinal convective rolls near the horizontal boundaries, where the unstable density stratification is formed due to no-slip boundary conditions.

A more complicated situation takes place when the temperature gradient is applied along a layer of binary liquid, in which the cross effects arising from the interaction between temperature and concentration fields can result in instability. It is shown [16–21] that, depending on the buoyancy ratio (ratio of solutal and thermal Rayleigh numbers), either thermoconcentration (double diffusive) or thermodiffusion (Soret effect) mechanisms are responsible for the onset of instability. The study of the advective flow induced solely by a concentration gradient has received less attention, though

---

<sup>\*</sup>alex\_mizev@icmm.ru<sup>†</sup>demin@psu.ru

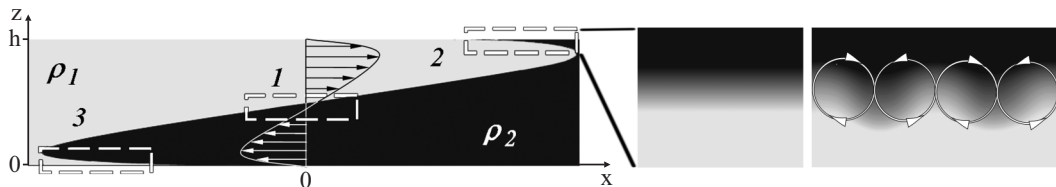


FIG. 1. Scheme illustrating the transition zone shape some time after the formation of the advective flow. Dashed rectangles denote the regions with stable (1) and unstable (2, 3) density stratification. Right frames show convective cell formation in the near-wall region.

such a problem statement is not meaningless. Isothermal mixing of layers with different densities is a frequent occurrence both in nature and in industry. This problem is not an analog to the problem of thermal advective flow from a hydrodynamic point of view. Essential differences in the characteristic times of heat and mass diffusion (Prandtl and Schmidt numbers differ by three orders of magnitude) can result in different instability scenarios. The experimental study of a solutal advective flow involves considerable difficulties because of the impossibility of maintaining a time-constant concentration gradient. Owing to relatively slow mass diffusivity, any initial concentration heterogeneity will be diffused rather fast through fluid motion. Only the nonstationary solutal advective flow can exist in this case. The exchange flow with two miscible fluids of different densities moving towards each other within a horizontal channel or a tube can be regarded as an example of this time-dependent situation. Buoyancy drives the denser fluid along the bottom wall, while the lighter fluid flows in the opposite direction at the top of the channel. This type of flow was studied in narrow channels [22,23] or in porous media [24–26]. In the course of these investigations it was found that, some time after the formation of the flow, the fluids spread as the square root of time when the viscous and buoyancy forces balance one another. To the best of our knowledge, the stability of this type of flow was not investigated.

In this paper, we present the results of an experimental and numerical study on the structure and stability of a solutal advective flow in a shallow horizontal layer. The flow is induced by the initial steplike density distribution which is formed when the vertically oriented shallow channel filled with a two-layer system of miscible fluids with stable density stratification is placed in a horizontal position. This leads to the appearance of a longitudinal density difference resulting in the development of advective flow (Fig. 1). The results demonstrate that the no-slip boundary conditions along the upper and lower horizontal boundaries cause the formation of near-wall layers with unstable density profile (see regions 2 and 3 in Fig. 1), which triggers the Rayleigh-Taylor instability in the form of longitudinal convective rolls. We have found that the solutal Péclet number, which indicates the relative strength of advection and diffusion, must exceed a critical value for the instability to set in. The spatiotemporal characteristics of the secondary flow, such as wavelength and formation time, are completely determined by the value of the Péclet number.

The paper is structured as follows. Section II contains the experimental part of the study. The structure and stability of the main flow are studied in Sec. II B. In Sec. II C, we discuss the physical mechanism of the observed instability and propose nondimensional parameters so that all the experimental results obtained for different substances and cuvettes can be represented by unified dependencies. The theoretical results and their comparison with the experimental data are presented in Sec. III. In conclusion (Sec. IV), we analyze some previous studies with similar flow structure, where the instability found is expected to take place.

## II. EXPERIMENTAL PART

### A. Experimental setup

The experiments were performed in a rectangular channel of 2.5 cm width and 10.0 cm length which was formed by two glass plates separated by a thin spacer giving a gap thickness of 0.12, 0.24

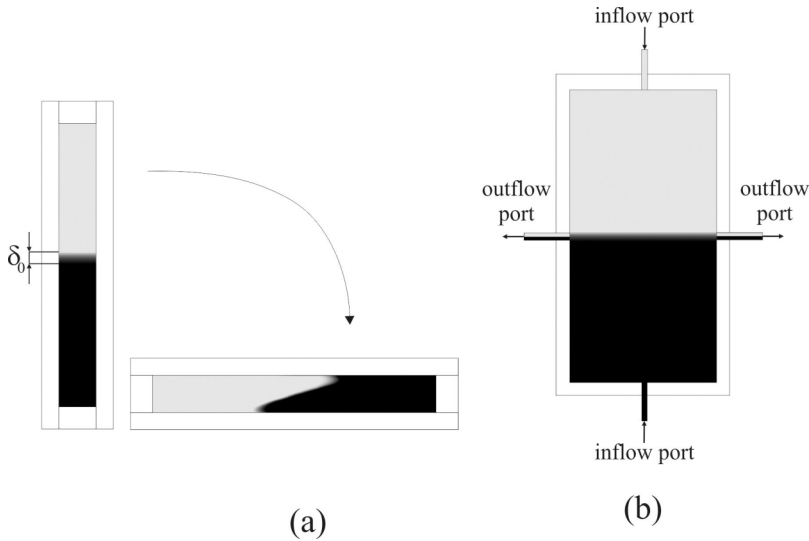


FIG. 2. Diagram illustrating the details of the experimental procedure. (a) The vertically oriented cuvette was initially filled with a two-layer system of miscible liquids with a stably stratified density profile. Setting the cuvette in a horizontal position resulted in a longitudinal steplike density distribution, which triggered the advective flow. (b) Scheme of the cuvette with two inflow and two outflow ports. The lighter liquid and the denser one entered from the upper and lower inflow ports, respectively. Two outflow ports located in the center of the sidewalls serve to divert the liquid from the mixing zone.

or 0.40 cm. Initially, the channel was vertically oriented and filled with a stably stratified two-layer system composed of water and an aqueous solution of well soluble substance [Fig. 2(a)]. To form an even transition zone, we applied the technique described in [27]. First, the cell was filled with water and then the lighter and denser liquids were flushed through the inflow ports located on the upper and lower boundaries, respectively [Fig. 2(b)]. The liquid from the mixing zone exited the cell through two central outflow ports. After the uniform, thin transition zone was formed, the inflow and the outflow were stopped. The initial thickness of the transition zone was  $0.20 \pm 0.03$  cm. Finally, the channel was placed in a horizontal position with a wide side upwards, which resulted in the development of an advective flow [Fig. 2(a)].

One layer was always a water layer, and the other was an aqueous solution of salt (sodium or potassium chloride, copper sulfate), alcohol (ethanol or isopropanol) or acetic acid. The use of different soluble substances and the change in their concentration allowed one to vary the density contrast  $\Delta\rho/\rho_0$  ( $\rho_0$  is the water density) from 0.003 to 0.080, the viscosity difference  $\Delta\eta$  between the layers from 0.01 to 2.22 cP, and the rate of diffusion of a solute through the water layer from 0.2 to  $2.0 \times 10^{-5}$  cm<sup>2</sup>/s. Some important characteristics of the solutions are given in Table I.

The parallel boundaries of the cuvette, illuminated by a collimated beam of monochromatic light, formed a Fizeau interferometer for visualization of refractive index inhomogeneities caused by the nonuniform distribution of the solute concentration. Additionally the interferometry allowed us to visualize the fluid motion. Owing to a small diffusion coefficient (order of  $1 \times 10^{-5}$  cm<sup>2</sup>/s), the concentration field is “frozen” in the moving fluid and so the evolution of the interference fringes contains information about the velocity and structure of the flow. The interference pattern observed through the wide side does not give us information about the concentration distribution across the channel, i.e., along the light beam. To reconstruct a three-dimensional (3D) structure of the concentration field, it is necessary to have a “side view” of the cuvette. Because of strong light refraction caused by a long optical path along the transverse size of the channel, side view interferometry in the main experimental cuvette is not possible. To visualize the concentration field

TABLE I. The properties of the aqueous solutions of different solutes used in the experiments:  $C_{\max}$  is the maximal mass concentration used in the experiments,  $\beta_c$  is the solutal expansion coefficient,  $(\Delta\rho/\rho_0)_{\max}$  is the density contrast ( $\rho_0$  is the water density) available at maximum concentration,  $\eta_{\max}$  is the viscosity at maximum concentration,  $k_\eta$  is the coefficient in the concentration dependence of viscosity  $\eta = \eta_0 + k_\eta C$  ( $\eta_0$  is the water viscosity), and  $D(C) = D_0 + k_D C$  is the concentration dependence of the diffusion coefficient.

Solute	$C_{\max}$	$\beta_c$	$(\Delta\rho/\rho_0)_{\max}$	$\eta_{\max}$ (cP)	$k_\eta$ (cP)	$D(C)$ (cm <sup>2</sup> /s)
NaCl	9	0.008	0.065	1.09	0.01	1.5
KCl	14	0.007	0.092	0.86	-0.01	1.9
CuSO <sub>4</sub>	6.7	0.011	0.068	1.34	0.05	0.7 - 0.03C
Ethanol	20	-0.002	0.030	2.00	0.05	1.0 + 0.003C
Isopropanol	40	-0.0015	0.067	3.40	0.06	1.2 - 0.03C
Acetic acid	20	0.0014	0.028	1.40	0.02	1.2 - 0.01C

and the flow structure in the second direction, an additional cuvette was made. Actually, it was the vertical cross section of the main channel. Two glass plates separated by a thin spacer formed the cavity of 9.0 cm length, 0.80 cm height, and 0.06 cm width. The experimental procedure was similar to that applied to the main cuvette. Initially, the vertically oriented cuvette was filled with a two-layer system, and further it was placed in a horizontal position with a wide side sideways. The side view of the concentration distribution was visualized using the Fizeau interferometer. Because of the essential difference in the geometries of the main and additional cuvettes, the interference patterns obtained for the latter were used for qualitative reconstruction of the 3D structure of a concentration field rather than for measurements.

### B. Structure and stability of the main flow

The interference pattern illustrating the concentration distribution some time after the channel has been set into a horizontal position is presented in Fig. 3. The transition zone between the layers which was initially oriented vertically is distorted by the flow. The form of this zone reflects the velocity profile of the advective flow, as the concentration field is “frozen” into the moving fluid. The inflection points of the transition zone, which correspond to a maximum velocity, are as well the front edges of the propagating layers. The coordinates of the front edges of the top and bottom layers correspond to the positions of the first interference fringe from the left and right side in the top view projection [Fig. 3(a)]. The transition zone and, hence, the velocity profile have a Z-shaped form, and the inflection points are appreciably shifted towards the horizontal boundaries due to the action of the buoyancy force, which has different signs in the upper and lower halves of the channel. The velocity profile is symmetric relative to the initial position of the interface. Unfortunately, the part of the transition zone located near the horizontal boundaries is not fully visible owing to the refraction [side view in Fig. 3(b)].

The typical time dependence of the front edge coordinate is presented in Fig. 4. The average of the coordinates of left and right edges was used since the layers moved symmetrically. It is seen that the flow is quasistationary as the front edge velocity becomes almost constant after a short transient period.

The results of the experiments showed that the main advective flow, presented in Fig. 3, became unstable when the density difference reached a certain threshold value, which depended on the solute used. Some time after the beginning of the fluid motion, two systems of longitudinal convective rolls appeared symmetrically relative to the initial position of the interface [Fig. 5(a)]. The side view projection [Fig. 5(b)] allowed us to reconstruct the structure of the secondary flow. The system of convective cells was formed in the areas adjacent to the upper and lower boundaries of the cavity. Note that the narrow size of the additional cavity did not allow the cells to orient along the flow as

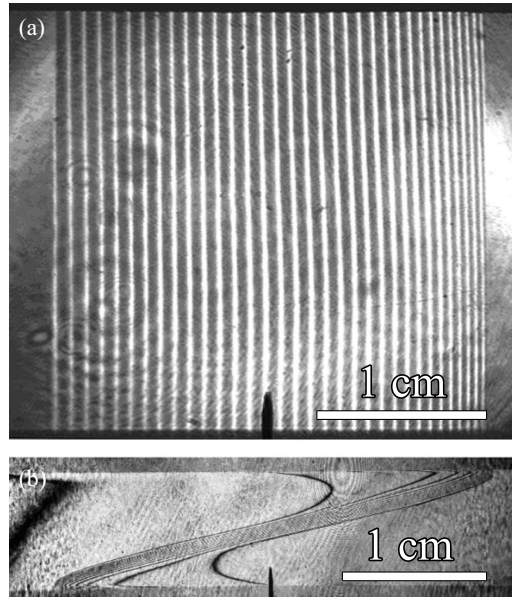


FIG. 3. (a) Top view and (b) side view of the stable advective flow obtained in the main and additional cuvettes, respectively. The same two-layer system composed of water and the aqueous solution of isopropanol with density contrast  $\Delta\rho/\rho_0 = 0.009$  was used in both cuvettes. The thickness of the main cuvette is  $h = 0.12$  cm. The black mark indicates the initial position of the contact area of liquids (see Supplemental Material at [28] for Movie V1.avi).

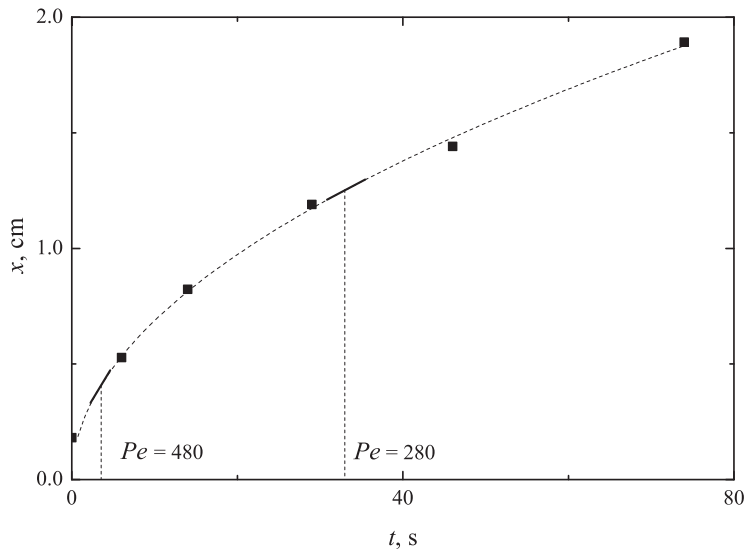


FIG. 4. Time dependence of the front edge coordinate for the system composed of water and the aqueous solution of NaCl with density contrast  $\Delta\rho/\rho_0 = 0.041$ . The channel thickness is  $h = 0.12$  cm. Two dashed lines mark the moments of time at which instability appears [left line,  $t = 4$  s; see Fig. 8(b)] and disappears [right line,  $t = 32$  s; see Fig. 8(d)]. The Péclet numbers shown near the lines were calculated for the mentioned moments of time.

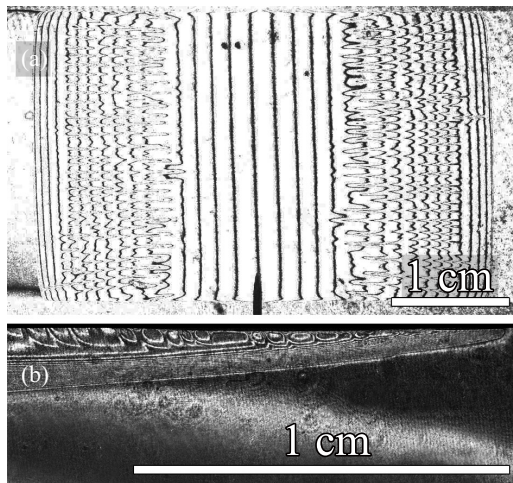


FIG. 5. (a) Top view and (b) side view of the unstable advective flow obtained in the main and additional cuvettes, respectively. The same two-layer system composed of water and aqueous solution of NaCl with density contrast  $\Delta\rho/\rho_0 = 0.046$  was used in both cuvettes. The thickness of the main cuvette is  $h = 0.12$  cm. The black label in the top view indicates the initial position of the contact area of liquids. Only the right front edge is presented in the side view to show a close-up of the secondary structure (see Supplemental Material [28] for Movies V2.avi and V3.avi).

in the main cavity. However, such an additional projection made it possible to localize the zones of instability in order to understand its mechanism discussed below.

The analysis of the results has revealed that the advective flow velocity increases with increasing density difference and cavity thickness and decreases when the viscosity of any layer increases. The results of all experiments obtained for different liquid pairs and different cavity thicknesses are described by the common dependence of the nondimensional coordinate on the nondimensional time:

$$X = \frac{x}{h}, \quad T = \frac{t}{\tau_v} \text{Gr}.$$

Here,  $h$  is the cavity thickness,  $\tau_v = h^2/\nu$  is the viscous diffusion time scale,  $\text{Gr} = g\Delta\rho h^3/\rho_0\nu^2$  is the Grashof number,  $\nu$  is the maximal kinematic viscosity in the fluid pair,  $\Delta\rho$  is the density difference, and  $g$  is the gravitational acceleration. A generalized dependence on these nondimensional coordinates is presented in Fig. 6(a). Open symbols refer to a situation when the main flow remained stable throughout the experiment. Shaded symbols correspond to the case of unstable advective flow. It is seen that the experimental points fall into two groups, which indicates different velocities of the main flow in stable and unstable cases. The best approximation is  $X = A\sqrt{T}$  with  $A = 0.075$  and  $A = 0.115$  for the cases of steady and unsteady advective flow, respectively.

The larger value of the coefficient  $A$  in the unstable case in comparison with the stable one can be interpreted at first sight as decreased drag due to the secondary flow. However, in fact the instability increases the drag, resulting in slowing down of the main flow. This is well seen from the front edge position evolution presented in dimensional form in Fig. 6(b). The fact that the unstable curve is located above the stable one in Fig. 6(a) is the result of nondimensionalization rather than decreasing the drag. The time is scaled by the molecular viscous time for both stable and unstable flow. However, in the latter case one needs to use an effective viscosity (like in the case of a turbulent flow) which is higher than the molecular one when the secondary flow exists. If we use this effective viscosity instead of the molecular one, then both curves (stable and unstable) will coincide, as they describe the same main flow, but with different viscous drag. Unfortunately, there is no way to measure the

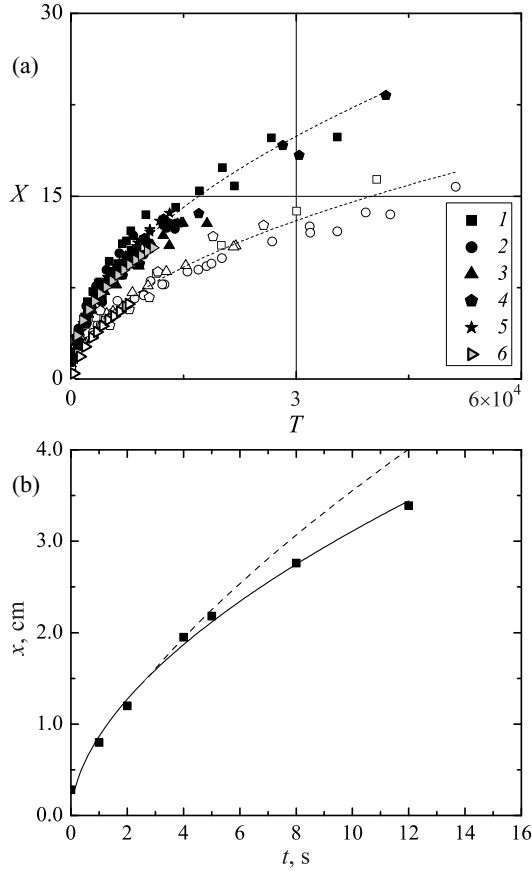


FIG. 6. (a) Dependence of the nondimensional front edge coordinate on the non-dimensional time for the water layer and the aqueous solution of (1) isopropanol, (2) NaCl, (3) acetic acid, (4) ethanol, and (5) copper sulfate. The results of numerical simulation are denoted by right-pointing triangles (6). Open and shaded symbols indicate the stable and unstable development of the advective flow, respectively. The dashed lines correspond to the best approximation in the form of  $X = A\sqrt{T}$  with  $A = 0.075$  and  $A = 0.115$  for steady and unsteady advective flows, respectively. (b) Time dependence of the front edge coordinate for the system of water and aqueous solution of NaCl with density contrast  $\Delta\rho/\rho_0 = 0.019$ . The channel thickness is  $h = 0.40$  cm. It is seen that the appearance of the secondary flow at  $t \approx 4$  s results in deceleration of the main flow.

effective viscosity in our experiments, and so we use the molecular viscosity to nondimensionalize the time in both cases.

### C. Secondary flow: Characteristics and physical mechanism

Further we discuss the physical mechanism responsible for the advective flow instability and the formation of the secondary convective structure in the near-wall region.

One of the possible mechanisms of the main flow instability might be viscous fingering [29] since one liquid displaces another of different viscosity. However, the viscous fingering is hardly the cause of the secondary flow observed. First, it should result in asymmetry of the structure; i.e., instability should arise only on one side, where the less viscous fluid displaces the more viscous one. Second, the viscous fingering instability should develop directly on the front edge, whereas the instability we observed arises far behind the front edge. Third, the typical wavelength of the viscous

fingering instability in the miscible case should be about five times the cuvette thickness, which is much higher than what we found in the experiments.

The absence of viscous fingering in our experiments can be explained as follows. Unlike the case of immiscible liquids, in which this instability develops at any viscosity ratio  $M = \eta_1/\eta_2$  (here,  $\eta_1$  and  $\eta_2$  are the viscosities of the displaced and displacing fluids) more than unity [29], the miscible displacement can remain stable even at higher values of this parameter. This was found experimentally for both rectilinear [30] and radial [31] miscible displacements in a Hele-Shaw cell. Lajeunesse *et al.* [30,32,33] and later Goyal *et al.* [34,35] revealed in their theoretical studies the critical viscosity ratio  $M_c = 3/2$  below which the interface is always stable. At large viscosity ratio the flow rate should exceed a certain threshold for the instability to occur. The viscosity ratio for most liquid pairs used in our experiments (see Table I) was less than the critical one. Exceptions are related to the solutions of ethanol and isopropanol, in which the viscosity ratio can exceed the critical one at high concentrations. However, the flow rate estimated by us for these experiments was at least one order of magnitude smaller than that predicted theoretically for development of the viscous fingering.

We offer here another instability mechanism. Figure 1 schematically shows a relative position of the layers some time after the beginning of the experiment. Two characteristic regions of the transition zone can be marked out: the first one is located between the inflection points in the middle part of the cavity and characterized by a stable density distribution, and the second (regions 2 and 3 in Fig. 1) is disposed in the near-wall regions and characterized by unstable density stratification (the denser liquid is situated above the less dense one). As a result, the Rayleigh-Taylor instability develops, which leads to the formation of convective cells. In this situation, the cells are formed against a background of the advective flow, which causes the secondary structure to occur in the form of longitudinal spiral rolls oriented along the main flow.

The obtained instability arose in a threshold manner and developed when the density difference between the layers reached a certain critical value, which was different for different solutes. This threshold development of the secondary structure looks rather strange because of the well-known fact that the Rayleigh-Taylor instability is not a threshold phenomenon. To explain this fact, it is reasonable to mention that the denser liquid layer located near the upper wall (or that of the less dense liquid located near the lower wall) is rather thin. If diffusion is fast enough, then these near-wall layers can be diffused prior to the onset of the Rayleigh-Taylor instability. However, the area of the transition zone increases and, therefore, the zone itself becomes thinner with time. Thus, there are two competing mechanisms which are capable of changing the thickness of the transition zone with different rates, thereby changing the conditions for the onset of the instability.

The ratio of the characteristic times of these two mechanisms is described by the solutal Péclet number  $Pe = uh/D$ , where  $u$  is the velocity of the advective flow and  $D$  is the diffusion coefficient of the solute. The higher the value of this dimensionless parameter, the lower is the contribution of the diffusion mechanism to density distribution blurring. Figure 7 shows a stability map for the advective flow in the Gr-Pe plane. The Péclet number is defined at the moment when the instability appears. If the main flow remains stable during the entire experiment, then the Péclet number is calculated from the maximum front velocity obtained in this experiment. It is seen that the instability (shaded symbols) develops when the Péclet number is greater than the critical value  $Pe^* \approx 300$  independently of the Grashof number. The flow remains stable at  $Pe < Pe^*$ .

The mechanism described above is confirmed indirectly by the following observations. In some experiments, the secondary structure developed in the beginning but disappeared later on. The time series of interferograms which illustrates this transition regime is presented in Fig. 8. The time evolution of the front edge position corresponding to this series is shown in Fig. 4. Such behavior is explained by the mechanism proposed above. Because the main flow is not stationary, its velocity is essentially varied, especially at the initial stage. This means that the Péclet number also changes until the quasistationary flow regime is established. At the initial stage the advective flow velocity (the local time derivative on the graph given in Fig. 4) and, therefore, the Péclet number are maximal. In the case when it is greater than the critical value, the instability develops [Fig. 8(b)].

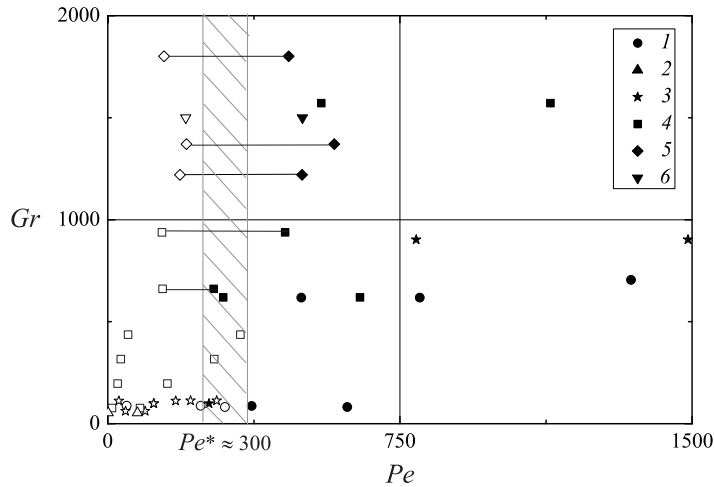


FIG. 7. The map of the stability of the advective flow in the Gr-Pe plane for water and the aqueous solution of (1) isopropanol, (2) acetic acid, (3) ethanol, (4) NaCl, and (5) KCl. The results of the numerical simulation are denoted by down-pointing triangles (6). Open and solid symbols indicate the stable and unstable development of the advective flow, respectively. The pairs of the experimental points connected by a line correspond to the transition regime, within which the initially developed instability disappears as the advective flow slows down. The data corresponding to the solid point in this pair are calculated for the moment when the secondary flow first appears on the interferogram [as in Fig. 8(b)]. The experimental data obtained for the moment when the secondary flow completely fades [as in Fig. 8(d)] were used to calculate the data corresponding to the open point in the pair.

Later, the decrease of the flow velocity gives rise to the reduction of the Péclet number. If it becomes smaller than the critical value, then the secondary structure will disappear [Fig. 8(d)]. In this case the system passes from the unstable region to the stable one in the Gr-Pe plane. The pairs of data points corresponding to such a transition regime are connected by the lines in Fig. 7. The right and left points in the pairs correspond to the moments when the secondary structure first appears on and fully disappears from the interferogram, respectively.

The analysis of the experimental data demonstrated that the wavelength  $\lambda$  of the secondary structure decreased with an increase of the density difference between the layers and with a decrease in the diffusion coefficient, but it almost did not change due to cavity thickness variation. All data obtained were represented by the dependence of the dimensionless wavelength  $\Lambda = \lambda/h$  on the Péclet number (Fig. 9). The best approximation is  $\Lambda \sim Pe^{-1/3}$ . Note that the flow velocity and, therefore, the Péclet number decreased with time, which resulted in slow wavelength increase.

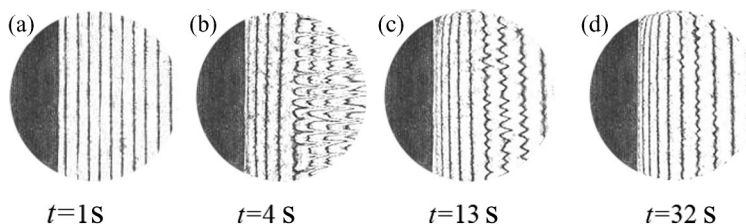


FIG. 8. Time series of interferograms illustrating the transition regime when the initially developing instability disappears as the advective flow slows down. The images presented correspond to the time evolution of the front edge coordinate shown in Fig. 4 (see Supplemental Material [28] for Movie V4.avi).

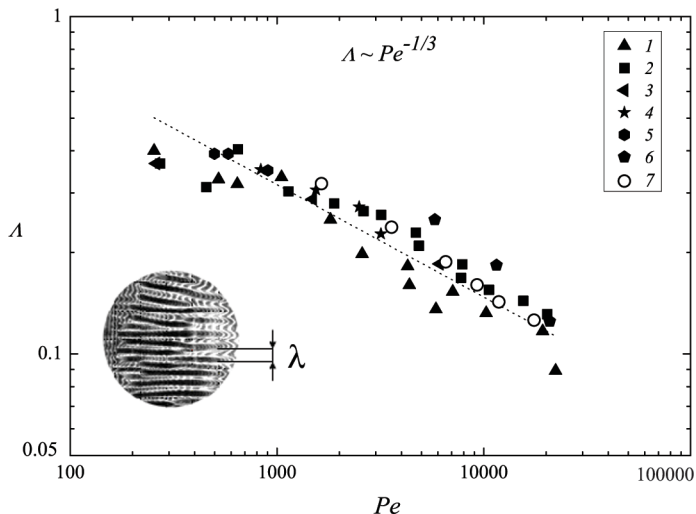


FIG. 9. Dependence of the nondimensional wavelength on the Péclet number for water and the aqueous solution of (1) isopropanol, (2) NaCl, (3) ethanol, (4) acetic acid, (5) KCl, and (6) copper sulfate. The results of the numerical simulation are given by open circles (7). The dashed line corresponds to the best approximation in the form of  $\Lambda \sim Pe^{-1/3}$ .

To avoid uncertainty, the dependence presented in Fig. 9 was obtained for the wavelength values measured at the moment when the instability sets in.

The study of the instability formation process has shown that the secondary structure needs some time to develop. To examine this in more detail, we measured the formation time  $t_f$  under different initial conditions. Formation time is the time measured from the moment when the channel was placed in a horizontal position to the moment when the secondary structure was first detected in the interferogram. The analysis of the experimental data demonstrated that  $t_f$  decreased as the cell thickness and the density difference increased and it increased as the viscosity grew (it refers to the highest viscosity between the pair of layers). The dependence of the dimensionless formation time  $T_f = t_f/\tau_v$  (here  $\tau_v = h^2/\nu$ , viscous diffusion time scale) on the Péclet number is shown in Fig. 10. The results of all experiments are described by the common dependence  $T_f \sim Pe^{-1}$  in these coordinates.

### III. THEORETICAL PART

Let us consider a rectangular cavity (Fig. 11), the horizontal dimensions of which are much longer than its thickness; i.e.,  $L, H \gg d$ . The cuvette is filled with an aqueous solution of a substance. The initial distribution of solute concentration provides a steplike density profile along the cuvette. This leads to the development of an advective flow in a gravity field. Assuming the isothermal conditions and small density changes due to concentration variations, the binary mixture convection is described by the system of equations written in Boussinesq approximation:

$$\begin{aligned} \frac{\partial \mathbf{V}}{\partial t} + (\mathbf{V}\nabla)\mathbf{V} &= -\frac{1}{\rho}\nabla p + \nu\Delta\mathbf{V} - g\beta_c C\boldsymbol{\gamma}, \\ \frac{\partial C}{\partial t} + (\mathbf{V}\nabla)C &= D\Delta C, \\ \operatorname{div}\mathbf{V} &= 0. \end{aligned} \tag{1}$$

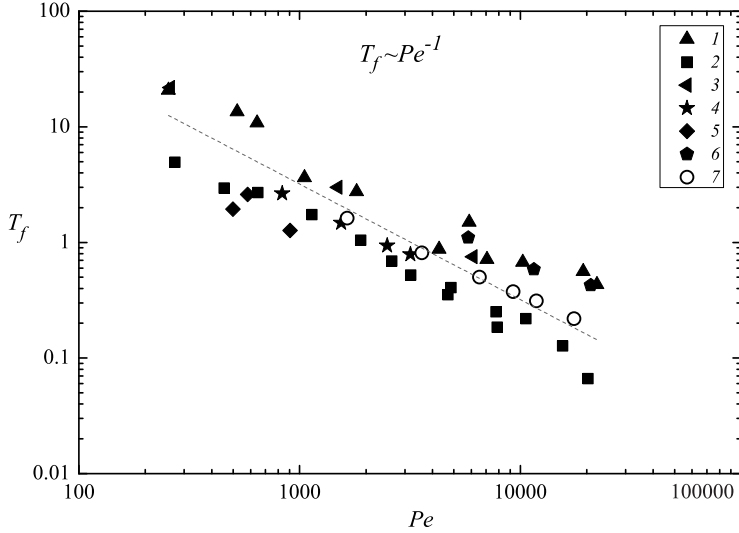


FIG. 10. Dependence of the nondimensional formation time of the secondary flow on the Péclet number for water and the aqueous solution of (1) isopropanol, (2) NaCl, (3) ethanol, (4) acetic acid, (5) KCl, and (6) copper sulfate. The results of the numerical simulation are denoted by open circles (7). The dashed line corresponds to the best approximation in the form of  $T_f \sim Pe^{-1}$ .

Here  $\mathbf{V}$ ,  $p$ ,  $\rho$ , and  $C$  are the dimensional velocity, pressure, density, and mass concentration of an admixture, respectively;  $\beta_c$  is the solutal expansion coefficient;  $g$  is the gravity acceleration; and  $\mathbf{y}$  is the unit vector directed vertically upwards. The coefficients of kinematic viscosity  $\nu$  and diffusion  $D$  are taken to be constant.

All the boundaries are rigid and impermeable:

$$\mathbf{V}|_{\Gamma} = 0, \quad \left. \frac{\partial C}{\partial \mathbf{n}} \right|_{\Gamma} = 0. \quad (2)$$

Here  $\mathbf{n}$  is the unit vector directed normally to the cavity boundary  $\Gamma$ .

Initially, the fluid is quiescent, and the solute concentration is given by

$$C = C_0[\text{erf}((H/2 - y)/l) + 1]/2, \quad (3)$$

where  $l$  is the parameter which describes the initial width of the transition zone considered in the experimental part of the paper.

The problem defined by Eqs. (1)–(3) was solved by the finite volume method through direct numerical simulations in dimensional form using the OPENFOAM package. The Euler implicit scheme

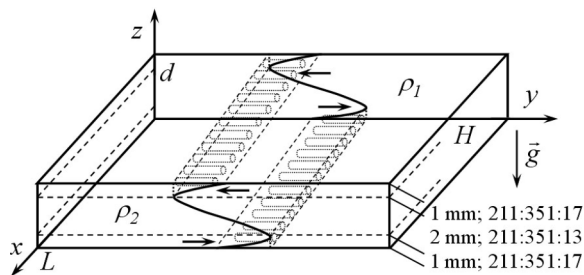


FIG. 11. Computational domain.

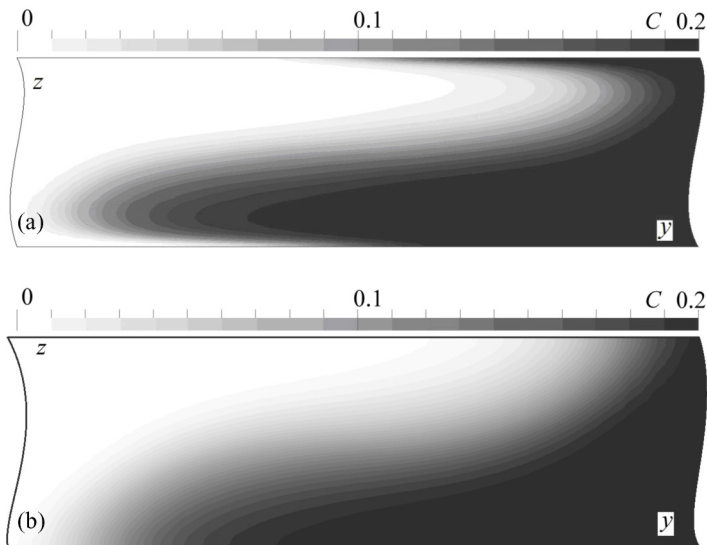


FIG. 12. Vertical cross section of the concentration field in the  $y$ - $z$  plane at  $x = L/2$  obtained in numerical simulations for the case of (a) no-slip and (b) free-slip boundary conditions on the upper and lower horizontal boundaries.

of the first-order accuracy was used for time derivatives, and the Gauss linear scheme of the second-order accuracy for spatial derivatives. A denser mesh was applied near the upper and lower boundaries, where the instability was found experimentally (Fig. 11). The simulations were made for the cavity with  $L = 0.24$  cm,  $H = 8$  cm, and  $d = 0.4$  cm using the following medium parameters:  $\nu = 1 \times 10^{-2}$  cm<sup>2</sup>/s,  $D = 1 \times 10^{-5}$  cm<sup>2</sup>/s, and  $\beta_c = 0.1$ .

In the case of small Péclet numbers, the advective flow is stable [see Figs. 6(a) and 7]. Figure 12(a) presents the vertical cross section of the concentration field in the  $y$ - $z$  plane at  $x = L/2$ . It is seen that the flow spreads symmetrically in both directions. Because of the no-slip boundary conditions, the denser liquid is above the less dense one near the upper and lower horizontal boundaries. Increase of the Péclet number leads to instability development in these regions [see Figs. 6(a) and 7]. Two vertical cross sections of the concentration field in the  $x$ - $z$  plane at  $y = 2$  cm and  $y = 6$  cm symmetrically located in relation to the initial position of the interface are presented in Figs. 13(a) and 13(b). One can observe the formation of a cellular convective structure in the near-wall regions, where the unstable density stratification takes place. The “top view” of the secondary flow structure is shown in Fig. 13(c). To improve comparison with the experimental results, the concentration distribution was averaged across the layer. It is seen that the cells are elongated in the flow direction, forming the secondary flow structure in the form of longitudinal spiral rolls oriented streamwise.

To verify the instability mechanism proposed above, we repeated simulations assuming free-slip boundary conditions on both horizontal rigid boundaries. The vertical cross section of the concentration field in the  $y$ - $z$  plane at  $x = L/2$  is presented in Fig. 12(b). We found that the change of the boundary conditions from no slip to free slip makes the formation of the instability impossible due to the absence of the unstable density distribution in the near-wall regions. The main flow remains stable even if the Péclet number exceeds the critical value by two orders of magnitude.

The comparison of the spatiotemporal characteristics of the main and secondary flows obtained numerically and during the laboratory experiment are presented in Figs. 6(a), 9, and 10. The results are in good quantitative agreement, which additionally supports the validity of the instability mechanism proposed in this paper.

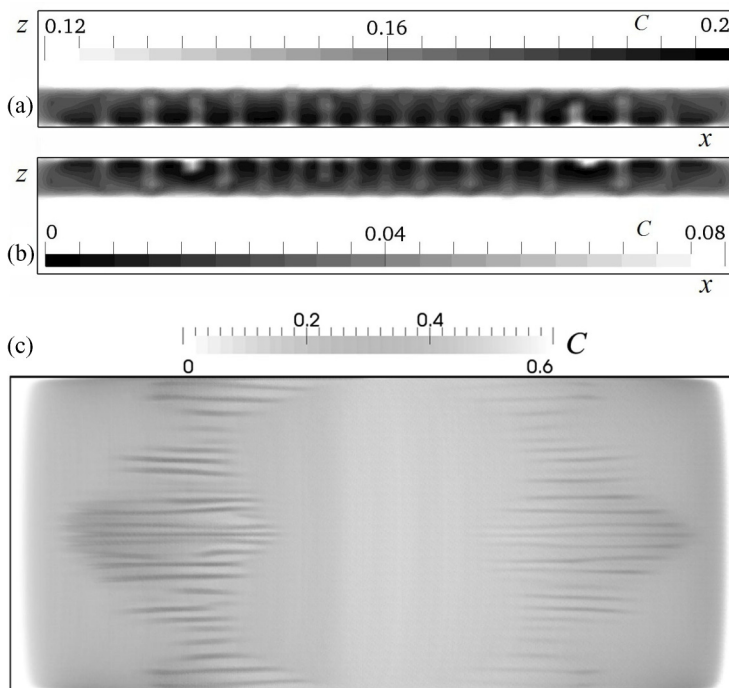


FIG. 13. Structure of the secondary flow obtained in numerical simulations. Vertical cross section of the concentration field in the  $x$ - $z$  plane at (a)  $y = 2$  cm and (b)  $y = 6$  cm symmetrically located relative to the initial position of the boundary between the fluids. (c) Top view of the flow structure obtained by averaging the concentration field across the layer.

#### IV. DISCUSSION AND CONCLUSIONS

We have presented an experimental and numerical study of the structure and stability of the solutal advective flow induced by the initial steplike density distribution caused by inhomogeneous solute concentration along a horizontal channel. It has been found that the main flow becomes unstable, which results in the appearance of longitudinal spiral rolls in the near-wall region. This phenomenon is associated with the Rayleigh-Taylor instability which develops near both the upper and lower horizontal boundaries. The unstable density stratification appears inside the transition zone separating the solutions due to no-slip boundary conditions. The temporal evolution of this zone is defined by advection, which stretches it, making it thinner, and by diffusion, which blurs it. The analysis of the obtained results has revealed that the solutal Péclet number, a measure of the relative strength of advection and diffusion, must exceed the critical value  $Pe^* \approx 300$  for the instability to set in. We have found that the Péclet number completely defines the spatiotemporal characteristics of the secondary flow. This allows us to represent all the experimental results obtained for different substances and cuvettes in the form of the unified dependence on this nondimensional parameter.

The comparison with the results obtained earlier for thermal advective flows [5–7,9–11] shows the universality of the instability found. In spite of different mechanisms of main flow generation (temperature or concentration gradient) and different rates of dissipative processes (heat diffuses two to three orders faster than mass), the same physical mechanism is responsible for the main flow instability. As in the solutal case, the unstable temperature stratification caused by no-slip boundary conditions in the upper and lower walls of a horizontal channel results in the Rayleigh-Taylor

instability at high enough Prandtl numbers. Hence, the longitudinal spiral rolls similar to those observed in the solutal case appear.

It is interesting to compare the results presented in the paper with the studies of the so-called exchange flow mentioned in Sec. I. This type of flow is certainly a kind of a solutal advective flow, and it is directly analogous to the flow studied here. Researchers usually focus on studying the shape of a transition zone between two fluids and its temporal evolution. The authors of the works studying the flow in Hele-Shaw cells [22,23] and in porous channels [24–26] have found that the front edges of a zone between two fluids spread as the square root of time; this is exactly the same as that in our study. The instability of the main flow has been only reported in [22]. The patterns observed there are very similar to those considered here, and their occurrence is also associated by authors with the formation of an unstable density profile due to no-slip boundary conditions (no detailed study of these structures has been done). In all other works considering the exchange flow, the main flow is found to be stable, which can be attributed to the fact that the values of the Péclet number are not high enough in these studies. Rather high viscosity of the fluids used in Hele-Shaw cells [23] or low permeability of porous media [24–26] resulted in very slow fluid motion which decreases this nondimensional parameter. The analysis of the above mentioned studies shows that the Péclet number is in the interval from  $10^{-1}$  to  $10^2$ , which is lower than the critical value  $Pe^* \approx 300$  found in our investigation and, therefore, is not enough for the development of the Rayleigh-Taylor instability.

Note that the instability found in this work should appear in all situations where a liquid moves along a horizontal solid wall displacing another miscible liquid with different density. With the no-slip boundary condition, the density gradient normal to the wall is generated. In the case when the denser liquid displaces the less dense one near the lower boundary or the less dense liquid displaces the denser one near the upper boundary, the density stratification is unstable, which creates the conditions for the development of the Rayleigh-Taylor instability. The review of the literature has shown that the situation described above takes place in intrusion flows [36,37], horizontal convection [38–41], gravity currents [42], and miscible displacement in a horizontal Hele-Shaw cell [43–46]. Instability of the main flow in the form of cellular convective patterns elongated streamwise was observed in all these studies. In miscible displacement, this instability can develop simultaneously with viscous fingering in the case when the less viscous fluid is injected into the more viscous one. In the reverse case when the system is viscously stable, the Rayleigh-Taylor mechanism is found to be the only one responsible for the main flow instability. In all studies, the patterns appear in a threshold manner. The velocity of the main flow and the channel thickness (in the case of displacement) must be large enough for the instability development. This indicates the significance of the Péclet number, which defines the conditions for instability occurrence and the spatiotemporal characteristics of the secondary flow.

#### ACKNOWLEDGMENTS

The study was supported by the Ural Branch of the Russian Academy of Science (Program No. 15-10-1-16).

- 
- [1] G. A. Ostroumov, *Free Convection under the Conditions of the Internal Problem* (State Publishing House, Technico-Theoretical Literature, Moscow-Leningrad, 1952) [translation NACA Technical Memorandum No. 1407 (1958)].
  - [2] J. E. Hart, Stability of thin non-rotating Hadley circulations, *J. Atmos. Sci.* **29**, 687 (1972).
  - [3] A. E. Gill, A theory of thermal oscillations in liquid metals, *J. Fluid Mech.* **64**, 577 (1974).
  - [4] P. Laure, Etude des mouvements de convection dans une cavité rectangulaire soumise à un gradient de température horizontal, *J. Mec. Theor. Appl.* **6**, 351 (1987).

- [5] J. E. Drummond and S. A. Korpela, Natural convection in a shallow cavity, *J. Fluid Mech.* **182**, 543 (1987).
- [6] H. P. Kuo and S. A. Korpela, Stability and finite amplitude natural convection in a shallow cavity with insulating top and bottom and heated from a side, *Phys. Fluids* **31**, 33 (1988).
- [7] T. M. Wang and S. A. Korpela, Convection rolls in a shallow cavity heated from a side, *Phys. Fluids. A* **1**, 947 (1989).
- [8] S. Someya, T. Munakata, M. Nishio, and K. Okamoto, Preliminary study of two immiscible liquid layers subjected to a horizontal temperature gradient, *J. Visualization* **6**, 21 (2003).
- [9] G. Z. Gershuni, E. M. Zhukhovitskii, and V. M. Myznikov, Stability of a plane-parallel convective flow of a liquid in a horizontal layer, *J. Appl. Mech. Tech. Phys.* **15**, 78 (1974).
- [10] G. Z. Gershuni, P. Laure, V. M. Myznikov, B. Roux, and E. M. Zhukhovitskii, On the stability of plane-parallel advective flow in long horizontal layers, *Microgravity Q.* **2**, 141 (1992).
- [11] G. Z. Gershuni, E. M. Zhukhovitskii, and V. M. Myznikov, Stability of plane-parallel convective fluid flow in a horizontal layer relative to spatial perturbations, *J. Appl. Mech. Tech. Phys.* **15**, 706 (1974).
- [12] M. G. Skafel, Thermal oscillations in low Prandtl number fluids, Ph.D. thesis, University of Cambridge, 1972.
- [13] J. E. Hart, Note on the stability of low-Prandtl-number Hadley circulations, *J. Fluid Mech.* **132**, 271 (1983).
- [14] D. T. J. Hurle, E. Jakeman, and C. P. Johnson, Convective temperature oscillations in molten gallium, *J. Fluid Mech.* **64**, 565 (1974).
- [15] B. Hof, On the onset of oscillatory convection in molten gallium, *J. Fluid Mech.* **515**, 391 (2004).
- [16] G. Z. Gershuni, A. V. Shalimov, and V. M. Myznikov, Plane-parallel advective binary mixture flow stability in a horizontal layer, *J. Heat Mass Transf.* **37**, 2327 (1994).
- [17] M. Ouriemi, P. Vasseur, A. Bahloul, and L. Robillard, Natural convection in a horizontal layer of a binary mixture, *Int. J. Therm. Sci.* **45**, 752 (2006).
- [18] T. P. Lyubimova, D. V. Lyubimov, D. A. Nikitin, and A. V. Perminov, Stability of the advective flow of a binary mixture in a horizontal layer with adiabatic boundaries, *C. R. Mec.* **341**, 483 (2013).
- [19] H. Han and T. H. Kuehn, Double diffusive natural convection in a vertical rectangular enclosure. I. Experimental study, *J. Heat Mass Transf.* **34**, 449 (1991).
- [20] Y. Kamotani, L. W. Wang, S. Ostrach, and H. D. Jiang, Experimental study of natural convection in shallow enclosures with horizontal temperature and concentration gradients, *J. Heat Mass Transf.* **28**, 165 (1985).
- [21] J. Lee, M. T. Hyun, and K. W. Kim, Natural convection in confined fluids with combined horizontal temperature and concentration gradients, *J. Heat Mass Transf.* **31**, 1969 (1988).
- [22] G. Matson and A. Hogg, Viscous exchange flows, *Phys. Fluids* **24**, 023102 (2012).
- [23] J. Martin, N. Rakotomalala, L. Talon, and D. Salin, Viscous lock-exchange in rectangular channels, *J. Fluid Mech.* **673**, 132 (2011).
- [24] M. L. Szulczewski and R. Juanes, The evolution of miscible gravity currents in horizontal porous layers, *J. Fluid Mech.* **719**, 82 (2013).
- [25] M. Dentz, D. M. Tartakovsky, E. Abarca, A. Guadagnini, X. Sanchez-Vila, and J. Carrera, Variable-density flow in porous media, *J. Fluid Mech.* **561**, 209 (2006).
- [26] H. E. Huppert and A. W. Woods, Gravity-driven flows in porous layers, *J. Fluid Mech.* **292**, 55 (1995).
- [27] S. Pringle, R. Glass, and C. Cooper, Double-diffusive finger convection in a Hele-Shaw cell: An experiment exploring the evolution of concentration fields, length scales and mass transfer, *Transp. Porous Media* **47**, 195 (2002).
- [28] See Supplemental Material at <http://link.aps.org/supplemental/10.1103/PhysRevFluids.2.103903> for movies.
- [29] P. G. Saffman, Viscous fingering in Hele-Shaw cells, *J. Fluid Mech.* **173**, 73 (1986).
- [30] E. Lajeunesse, J. Martin, N. Rakotomalala, and D. Salin, 3D Instability of Miscible Displacement in a Hele-Shaw Cell, *Phys. Rev. Lett.* **79**, 5254 (1997).
- [31] I. Bischofberger, R. Ramachandran, and S. Nagel, Fingering versus stability in the limit of zero interfacial tension, *Nat. Commun.* **5**, 5265 (2014).
- [32] E. Lajeunesse, J. Martin, N. Rakotomalala, D. Salin, and Y. Yortsos, Miscible displacements in a Hele-Shaw cell at high rates, *J. Fluid Mech.* **398**, 299 (1999).

- [33] E. Lajeunesse, J. Martin, N. Rakotomalala, D. Salin, and Y. Yortsos, The threshold of the instability in miscible displacements in a Hele-Shaw cell at high rates, *Phys. Fluids* **13**, 799 (2001).
- [34] N. Goyal and E. Meiburg, Miscible displacements in Hele-Shaw cells: Two-dimensional base states and their linear stability, *J. Fluid Mech.* **558**, 329 (2006).
- [35] N. Goyal, H. Pichler, and E. Meiburg, Variable-density miscible displacements in a vertical Hele-Shaw cell: Linear stability, *J. Fluid Mech.* **584**, 357 (2007).
- [36] W. Schöpf and O. Stiller, Three-Dimensional Patterns in a Transient, Stratified Intrusion Flow, *Phys. Rev. Lett.* **79**, 4373 (1997).
- [37] S. E. Norris, Rayleigh-Bénard roll formation in a thermal intrusion, in *Proceedings of the 18th Australasian Fluid Mechanics Conference*, edited by P. A. Brandner and B. W. Pearce (Australasian Fluid Mechanics Society, Launceston, Australia, 2012).
- [38] G. O. Hughes and R. W. Griffiths, Horizontal convection, *Annu. Rev. Fluid Mech.* **40**, 185 (2008).
- [39] J. C. Mullarney, R. W. Griffiths, and G. O. Hughes, Convection driven by differential heating at a horizontal boundary, *J. Fluid Mech.* **516**, 181 (2004).
- [40] G. J. Sheared and M. P. King, Horizontal convection: Effect of aspect ratio on Rayleigh number scaling and stability, *Appl. Math. Model.* **35**, 1647 (2011).
- [41] V. G. Batalov, A. N. Sukhanovskii, and P. G. Frik, Experimental investigation of helicoidal rolls in an advective flow over a hot horizontal surface, *Fluid Dyn.* **42**, 540 (2007).
- [42] D. Snyder and S. Tait, A flow-front instability in viscous gravity currents, *J. Fluid Mech.* **369**, 1 (1998).
- [43] F. Haudin, L. A. Riolfo, B. Knaepen, G. M. Homsy, and A. De Wit, Experimental study of a buoyancy-driven instability of a miscible horizontal displacement in a Hele-Shaw cell, *Phys. Fluids* **26**, 044102 (2014).
- [44] L. Talon, N. Goyal, and E. Meiburg, Variable density and viscosity, miscible displacements in horizontal Hele-Shaw cells. Part 1. Linear stability analysis, *J. Fluid Mech.* **721**, 268 (2013).
- [45] M. O. John, R. M. Oliveira, F. H. C. Heussler, and E. Meiburg, Variable density and viscosity, miscible displacements in horizontal Hele-Shaw cells. Part 2. Nonlinear simulations, *J. Fluid Mech.* **721**, 295 (2013).
- [46] P. Garik, J. Hetrick, B. Orr, D. Barkey, and E. Ben-Jacob, Interfacial Cellular Mixing and a Conjecture on Global Deposit Morphology, *Phys. Rev. Lett.* **66**, 1606 (1991).